The Intrinsically Unstructured Domain of PC4 Modulates the Activity of the Structured Core through Inter- and Intramolecular Interactions†

Hendrik R. A. Jonker,* Rainer W. Wechselberger, Rolf Boelens, Rob Kaptein, and Gert E. Folkers*

Bijvoet Center for Biomolecular Research, Section NMR Spectroscopy, Utrecht University, Padualaan 8, 3584 CH, Utrecht, The Netherlands

Received December 12, 2005; Revised Manuscript Received March 3, 2006

ABSTRACT: Proteins frequently contain unstructured regions apart from a functionally important and well-conserved structured domain. Functional and structural aspects for these regions are frequently less clear. The general human positive cofactor 4 (PC4), has such a domain organization and can interact with various DNA substrates, transcriptional activators, and basal transcription factors. While essential for the cofactor function, structural and functional knowledge about these interactions is limited. Using biochemical, nuclear magnetic resonance (NMR), and docking experiments, we show that the carboxy-terminal structured core domain (PC4ctd) is required and sufficient for binding to single-stranded DNA (ssDNA), double-stranded DNA (dsDNA), and the herpes simplex virion protein 16 (VP16) activation domain (VP16ad). We determined the interaction surfaces within PC4 and showed that VP16 and DNA binding are mutually exclusive. Although the amino-terminal domain of PC4 (PC4ntd) alone is devoid of any bioactivity, it increases the interaction with VP16ad. While it decreases the ssDNA-binding and DNA-unwinding activity, it does not influence dsDNA binding. Structural characterization of this domain showed that it is highly flexible and mostly unstructured both in the free form and in the complex. NMR titration experiments using various protein and DNA substrates of the individual domains and the full-length PC4 revealed local conformational or environmental changes in both the structured and unstructured subdomains, which are interpreted to be caused by inter- and intramolecular interactions. We propose that the unstructured PC4ntd regulates the PC4 cofactor function by specific interactions with the activator and through modulation and/or shielding of the interaction surface in the structured core of PC4ctd.

The current view on structure−function relationships is dominated by the central dogma that a well-defined three-dimensional structure is a prerequisite for biological function. Attempts to determine the structure of many cellular regulator proteins, including transcription activation domains of various transcription factors, showed that also the absence of a structure is essential for its biological function. Indeed, database predictions revealed that over 30% of all of the eukaryotic proteins contain consecutive disordered stretches of more than 40 amino acids. The presence of proteins, protein domains, or stretches of (low complexity) sequences that are unfolded in solution or adopt a nonglobular conformation led to the notion that the structure−function paradigm needs revision (*1*). This raises the question of how such intrinsically unstructured proteins (IUPs)[1] fulfill their functions. One assumption is that these IUPs adopt a more structured conformation upon interactions with a target (e.g., protein and DNA). However, accumulating evidence suggests that the biological function of a protein can also be performed in the disordered state. This led Dunker et al. (*2*) to propose a protein trinity, in which a protein can adopt an ordered structure, molten globules, or random-coil conformation, where the function depends upon any of these conformations or the transitions between them. Low complexity sequences are frequently found in proteins involved in transcription, and they are therefore frequently used to elucidate the mechanism underlying the function of proteins that lack any structure.

Transcription of eukaryotic class II genes involves a concerted action of the general transcription factors (GTFs) in the formation of a preinitiation complex (PIC) on the TATA-box promoter region. The assembly of the PIC is facilitated and regulated by a number of transcriptional activators and coactivators (*3*−*5*). Cofactors (or co-activators) mediate interactions between the general transcription machinery and DNA-bound activators to enhance or repress transcription (*6*−*8*). The transcriptional human positive

† This work is supported by financial assistance from the Netherlands Organization for Scientific Research (NWO).

* To whom correspondence should be addressed. E-mail: henry@vinden.nl. Telephone: +49-(0)69-798-29137. Fax: +49-(0)-69-798-29515 (H.R.A.J.); E-mail: g.folkers@chem.uu.nl. Telephone: +31-(0)30-253-9930. Fax: +31-(0)30-253-7623 (G.E.F.).

[1] Abbreviations: CSI, chemical-shift index; GST, glutathione *S*-transferase; GTF, general transcription factor; HSQC, heteronuclear single-quantum coherence; IUP, intrinsically unstructured protein; NOE, nuclear Overhauser enhancement; NOESY, NOE spectroscopy; PC4, human positive cofactor 4; PC4ntd or PC4ctd, amino- or carboxy-terminal domain of PC4; PIC, preinitiation complex; PSSI, probability-based secondary-structure identification; TAD, transcription activation domain; SEAC, serine- and acidic-rich region of PC4ntd; TALOS, torsion angle likelihood obtained from shift and sequence similarity; TAFII, TBP-associated factor; TBP, TATA-box binding protein; TFII, transcription factor II; TOCSY, total correlation spectroscopy; VP16, herpes simplex virion protein 16; VP16ad, activation domain of VP16.

10.1021/bi052531b CCC: $33.50
Published on Web 03/25/2006

cofactor 4 (PC4), mediates activator-dependent transcription by increasing the recruitment of the GTFs (*9*) and probably also RNA polymerase II through concerted interactions with the basal transcription machinery (*10*, *11*). Because PC4 stimulates activation of RNA polymerase II transcription by a wide variety of transactivation domains [herpes simplex virion protein 16 (VP16), AH, CTF, SP1, E1a, IE, and NF-κB], representing all major classes of transactivation domains (such as acidic, proline rich, or glutamine rich), it is considered to be a general cofactor (*12*, *13*). The ability to mediate activator-dependent transcription has been correlated to its capability to bind double-stranded DNA (dsDNA) (*9*). Contrary to transcriptional activation, PC4 has been shown to repress transcription under specific conditions (*11*, *14*) depending upon the interaction with melted dsDNA, hereafter referred to as bubble DNA (*15*). The inhibitory activity can be attenuated by the combined effects of TATA-box binding protein (TBP)-associated factors (TAFIIs), transcription factor II (TFII)H, and a preassembled RNA polymerase II holoenzyme (*11*, *14*−*17*). The helicase activity of ERCC3 (also referred to as XPB), present in TFIIH, is probably crucial for alleviation of PC4-mediated repression (*18*). Accordingly, the foremost function of PC4 could actually be to repress transcription until PIC assembly is complete, because TFIIH is generally believed to be the last factor to enter the PIC (*4*). Apart from its role in PIC stabilization and transcription regulation, PC4 is possibly involved in mRNA processing through the interaction with the polyadenylation factor CstF-64 (*19*), DNA replication by interactions with the replication factor RPA (*20*), and tumor suppression by interactions with the breast- and ovarian-specific tumor suppressor protein BRCA1 (*21*) and the proline- and glutamine-rich activation domains of AP-2 (*22*).

PC4 is composed of two domains with distinct functional properties and is highly conserved among higher eukaryotes (*23*−*25*). Transcriptional repression correlates with single-stranded DNA (ssDNA)-binding activity present in the carboxy-terminal half of PC4 (PC4ctd, residues 61−126), showing a preferential interaction with bubble DNA (*15*). The structure of the PC4ctd core domain has been elucidated by crystallography and revealed a homodimeric fold with two symmetrical β channels running in opposite direction (*26*). The ssDNA-binding surface of this domain has been identified by nuclear magnetic resonance (NMR) (*27*). The amino-terminal half of PC4 (PC4ntd, residues 1−60) comprises a serine- and acidic-rich region (SEAC), a lysine-rich region, and another region, rich in serine residues. It has been reported that two lysine residues can be acetylated by the cofactor p300, which increases the dsDNA-binding affinity by 40% (*28*). Furthermore, this lysine-rich region is shown to be important for the ability of PC4 to inhibit cdk1-, cdk2-, and cdk7-mediated phosphorylation of RNA polymerase II (*29*), an event thought to be critical in the onset of transcriptional elongation (*30*). The SEAC can be phosphorylated, which negatively regulates the cofactor function but not the ssDNA-binding activity of PC4 (*9*, *31*). Because of its ssDNA-binding properties and the inability to inhibit phosphorylation of RNA polymerase II (*29*) in its predominant phosphorylated form (*31*), PC4 may have a role in the conversion to the elongation phase of transcription (*18*).

The involvement of PC4ntd in the interactions with transcription factors or DNA is poorly studied despite the fact that phosphorylation of the SEAC modulates cofactor function. To better understand the contribution of this domain to the cofactor function, we investigated the structural and functional properties and involvement in activator and DNA binding. We have determined the PC4 interaction surfaces for the VP16 activation domain (VP16ad) and DNA by NMR, site-directed mutagenesis, and docking. Our results show that the PC4ctd interaction surface for VP16ad partially overlaps with the ssDNA-binding surface, which is also required for the unwinding activity. Although the lysine-rich region, shown to be involved in the interaction with VP16ad, exhibits a propensity to form secondary-structure elements, PC4ntd is highly flexible and mostly unstructured both in the complex and in the free form. Furthermore, the modulatory role of the lysine-rich region in PC4ntd is underscored by an increase in DNA-binding and DNA-unwinding activity by both deletion of the whole amino terminus and mutation of specific positive-charged residues. This led us to propose that unstructured regions could perform a regulatory role on the core of the protein by modulating the binding properties of the structured domain through transient inter- or intramolecular interactions.

MATERIALS AND METHODS

Preparation of Plasmids and Mutants. Glutathione *S*-transferase (GST)−VP16ad, PC4, PC4 deletion constructs, and the β2−β3 mutant (F76A,K77G,K79G) were kindly provided by S. Werten. GST−hRARβ AF1 (1−76), AF2 (137−448), and GST−E1A (121−187) have been described before (*32*). GST−SP1 (139−250) and GST−Oct1 (175−269) were polymerase chain reaction (PCR)-amplified using the expression vectors pSG5 SP1 and pSG5 Oct1 as templates, respectively. Primers have been extended with an *Eco*RI and *Nde*I restriction site at the 5′ end of the forward primer and a stop codon followed by an *Eco*RI site at the 5′ end of the reverse primer. PCR products were digested with *Eco*RI and cloned in the *Eco*RI site of pGEX3X or pGEX2T (APB).

The PC4 mutants were made by PCR with pet11a PC4 as a template using either a forward primer (F1) (gcggatcccatatgCCTAAATCAAAGGAACTTG) or reverse primer (R1) (cgggaattctcaCAGCTTTCTTACTGCG) together with mutant primers that simultaneously introduce restriction sites for convenient screening of mutants. Primers were extended so that the final PCR product contains suitable restriction sites for cloning. K67G and A47G,L48G were made using a two-step PCR reaction. Mutant forward and reverse primers were used together with the above-described reverse and forward primers, respectively, in separate tubes. This was followed by a PCR reaction using the two PCR products plus the forward and reverse primer. The PCR product was, after digestion with *Nde*I and *Eco*RI, cloned in the corresponding sites of pET-11a PC4. Mutants K22G,K23G, K25G,R26G, K27G,K28G, K34G, and K37G,K38G were PCR-amplified with a mutant forward primer and reverse primer R1 and after digestion with *Hin*cII and *Eco*RI cloned in the *Hin*cII (partially digested) *Eco*R1-digested pET-11a PC4 plasmid. R85G was PCR-amplified with a mutant reverse primer and forward primer F1, and the PCR product was cloned after digestion with *Nde*I and *Bam*HI in the corresponding sites of pET-11a PC4. V20G was PCR-amplified using a megaprimer procedure. In the first PCR

reaction, a forward primer F1 and a reverse mutant primer were used. This PCR product, together with reverse primer R1, was used to generate the mutant PCR product. After digestion with *Nde*I and *Eco*RI, this fragment was cloned in pET-11a PC4, digested with these enzymes. The mutants R74G, K77G, and K79G were amplified with a mutant forward primer and reverse primer R1. After digestion of the PCR products with *Rsa*I and *Eco*R1, the fragments were cloned in pET-11a PC4 digested with *Rsa*I (partial digest) and *Eco*RI. The same procedure was used for K100G, using *Bam*HI and *Eco*RI to introduce the mutation in PET-11a PC4. Sequences of the used oligonucleotides for the PCR reactions are available upon request. All mutations have been confirmed by sequencing the full-length PC4 fragment.

Preparation of PC4. The PC4 proteins were prepared essentially as described by Werten et al. (*27*, *33*). Labeled (^{15}N,^{13}C) protein was obtained by using 0.5 g/L $^{15}NH_4Cl$ (Isotec) and either 4.0 g/L ^{12}C-glucose or 2.0 g/L ^{13}C-glucose (Isotec) in minimal media (4.4 g/L KH_2PO_4, 10.4 g/L $K_2HPO_4 \cdot 3H_2O$, 50 mg/L $MgSO_4 \cdot 7H_2O$, 7 mg/L Mohr's salt, 10 mg/L thiamine, and 50 mg/L ampicillin). The cells were harvested 3 h after induction with 1 mM isopropyl-β-D-thiogalactopyranoside (IPTG), resuspended in lysis buffer containing 20 mM Tris-HCl (pH 7.3), 500 mM KCl, 1% Triton X-100 [octylphenol-poly(ethylene glycol) ether], 10% glycerol, 1 mM ethylenediaminetetraacetic acid (EDTA), 2 mM DTT (1,4-dithiothreitol), 1 mM PMSF (phenylmethylsulfonylfluoride), and Complete protease inhibitor (Roche), freeze−thawed (−80 °C, twice) and sonicated (until 10% of the initial OD_{600} value). The lysate was cleared by centrifugation (45 min at 16 000 rpm, 4 °C), diluted to 200 mM KCl with a 20 mM Tris-HCl (pH 7.3) buffer containing 10% glycerol, 1 mM EDTA, 1 mM DTT, and 0.2 mM PMSF, loaded on a fast-flow Heparin Sepharose column (APB), and eluted with 500 mM KCl in the same Tris buffer. Selected fractions were diluted to 300 mM KCl with a 20 mM phosphate buffer (pH 6.0) containing 100 mM KCl and 1 mM DTT, applied on a CM-Accell cation-exchange column (Waters) and eluted by a linear salt gradient from 300 mM to 1 M KCl in the same phosphate buffer. If the sample did not appear as a single band on Coomassie-stained sodium dodecyl sulfate (SDS)−polyacrylamide gels, an additional purification was performed using a HiLoad Superdex-75 column (APB) with the same phosphate buffer containing 400 mM KCl.

The GST−PC4ntd fusion protein (kindly provided by P. C. van der Vliet) was cultured, purified, and cleaved with thrombin as described below for GST−VP16ad. After dialysis in 20 mM potassium-phophate buffer (pH 6.0) containing 100 mM KCl and 1 mM DTT, PC4ntd was further purified using a CM-Accell cation-exchange column (Waters) with a linear salt gradient from 100 mM to 1 M KCl in the same buffer.

Preparation of VP16ad. The GST−VP16ad (412−490) construct was kindly provided by S. Werten, overexpressed in *Escherichia coli* strain BL21(DE3)pLysS, and grown at 37 °C in LB media containing 50 μg/mL ampicillin and 40 μg/mL chloramphenicol. The cells were harvested 2 h after induction with 1 mM IPTG and resuspended in lysis buffer containing 50 mM Tris-HCl (pH 8.0), 250 mM KCl, 0.2% Triton X-100, 1 mM EDTA, 1 mM DTT, and Complete protease inhibitor (Roche). After freeze−thawing, sonication, and centrifugation, the supernatant was diluted 2.5 times with 50 mM Tris-HCl (pH 8.0) buffer containing 250 mM KCl, 0.2% Triton X-100, 1 mM EDTA, and 1 mM DTT, loaded on a Glutathione Sepharose 4B column (APB), and eluted with 10 mM glutathione in 50 mM Tris-HCl (pH 8.0) buffer with 50 mM NaCl. The GST moiety was removed using 100 units of thrombin (Sigma) per liter of bacterial culture in the same buffer supplemented with 2.5 mM $CaCl_2$ and 1 mM DTT. The sample was diluted to 20 mM NaCl with a 50 mM Tris-HCl (pH 7.0) buffer containing 1 mM EDTA, 1 mM DTT, and 1 mM PMSF and applied on a fast-flow Q-Sepharose column (APB). GST and VP16ad were separated using a linear gradient from 20 mM to 1 M NaCl in the same Tris buffer. If necessary, an additional gel filtration was performed as described above for PC4.

Protein Quantification. For the biochemical experiments, protein concentrations were determined by UV measurements, taking the calculated extinction coefficient at 280 nm for PC4 (13940 M^{-1} cm^{-1}). Alternatively, the amount was estimated using Coomassie-stained SDS−polyacrylamide gels. The protein concentrations were calculated relative to proteins with a known concentration using a GS-710 calibrated imaging densitometer (Biorad).

Electrophoretic Mobility Shift Assays (EMSAs). The oligonucleotides were purchased from Invitrogen. The bubble consists of 5′-GGGCGGCGGGTTTTTTTTGGCGGGGCGG and 5′-CCGCCCCGCCTTTTTTTTCCCGCCGCCC. For ssDNA binding, either of these strands was used; they both show essentially identical results. For dsDNA binding, a HIV/ML hybrid promoter fragment (*9*) was used. One strand was end-labeled with $^{32}P_\gamma$ATP using T4-kinase and subsequently purified from a polyacrylamide gel. An equimolar amount of unlabeled ssDNA was added to the gel-purified ssDNA for preparation of the various substrates, if required. Binding reactions were performed according to Werten et al. (*33*) in 20 μL of buffer containing 10 mM Tris-HCl (pH 7.3), 200 mM KCl, 5% glycerol, 1 mM EDTA, 1 mM DTT, and 10 μg/mL bovine serum albumin (BSA), together with the indicated amount of protein. After the addition of 500−5000 cpm of purified DNA (specific activity = 5×10^7 cpm/μg), samples were incubated for 2 h on ice and loaded on a prerun 7.5% polyacrylamide gel (29:1) containing 0.5 × TBE [Bio-Rad, mix for 89 mM Tris-HCl (pH 8.3), 89 mM boric acid, and 2 mM EDTA] as a running buffer. The dsDNA-binding experiments were loaded on a 6−7.5% polyacrylamide gel containing 0.5 × TBE with 0.1% Nonidet P40 [nonylphenylpoly(ethylene glycol)] added to both the gel and running buffer. The electrophoresis was carried out at 150 V for 2−4 h at 4 °C. Gels were vacuum-dried and exposed against a phosphor-imager screen for 1−5 days. Quantification was performed using a Molecular Imager FX system using the software Quantity One (Bio-Rad). The apparent K_d was determined by fitting the binding data using a nonlinear regression against the bound fraction $= 1/(1 + (K_d/[\text{protein}])^n)$, where n represents the Hill coefficient. For binding to ssDNA or bubble DNA, this coefficient appeared to be approximately 1 (1.1 ± 0.2), while for dsDNA, $n > 1$ (1.8 ± 0.4), indicating cooperative binding most likely because of the formation of a higher order complex. Binding affinities were determined by calculating the average K_d and standard deviation of at least three EMSA experiments. DNA binding in the presence of VP16 at the indicated concentra-

tions was performed by the addition of VP16 to PC4 in three ways: 1 h before, at the same time, or 1 h after the addition of labeled DNA. Identical results were obtained irrespective of the order of addition of VP16 and DNA to PC4. These binding assays were performed in 20 mM potassium phosphate buffer (pH 6.2), 50 mM KCl, 5% glycerol, 1 mM EDTA, 1 mM DTT, and 10 μg/mL BSA, because under high-salt conditions, the interaction between PC4 and VP16 was dramatically weakened.

Unwinding Assays. Unwinding assays were performed as described by Werten et al. (*33*) in a buffer containing 50 mM Tris-HCl (pH 7.5), 4% glycerol, 1 mM DTT, 10 ng/μL BSA, and the indicated amount of protein diluted in the same buffer. Reactions were started by the addition of the above-described bubble as a probe (1000 cpm) and incubated at 30 °C for 90 min. The reaction was stopped by the addition of 2.5 μL of 0.5× TBE containing 20% glycerol and 0.9% SDS and loaded immediately on a prerun 10% polyacrylamide gel in a 0.5× TBE buffer containing 0.1% SDS. The gels were subsequently treated and analyzed as described above. For inhibition of unwinding by VP16ad, a PC4−VP16ad complex was allowed to form for at least 30 min prior to the addition of the substrate to the reaction.

GST Pull-Down Assays. GST-fusion proteins were isolated from 50 mL cultures, and lysis was performed as described for VP16, while purification was performed in a batch at 4 °C according to the instructions of the supplier (APB). The GST beads were extensively washed with 50 mM Tris-HCl (pH 8.0) containing 50 mM NaCl and subsequently 3 times with 20 mM potassium phosphate buffer (pH 6.2) and 50 mM KCl. Binding experiments were performed in 200−800 μL of binding buffer [20 mM potassium phosphate buffer (pH 6.2) containing 50 mM KCl, 0.2 mM PMSF, and 1 mM DTT and supplemented with 0.2 μg/μL BSA] with 2 μg of GST−VP16 bound to GST beads in the presence of the indicated amount of PC4. Reaction mixtures were incubated for 2 h at 20 °C and washed 4 times with 500 μL of binding buffer. Dry GST beads were resuspended in SDS sample buffer and loaded on a 12.5% SDS−polyacrylamide gel. To compare binding affinity, 10% of the total input of the binding reaction was loaded on the SDS−polyacrylamide gel next to the GST pull-down experiments. The influence of dsDNA or ssDNA on the interaction between PC4 and VP16 was tested by the addition of the indicated concentrations of DNA either 1 h before or 1 h after the addition of GST−VP16ad to the reaction mixture containing PC4. A similar decrease in the interaction between GST−VP16ad and PC4 was obtained irrespective of the order of addition of DNA to the reaction.

NMR Spectroscopy. The NMR samples were exchanged toward a buffer, containing 50 mM KCl (400 mM for PC4ctd to avoid aggregation), 50 mM phosphate buffer (pH 5.6), and Complete protease inhibitor (Roche), by repeated dilution and concentration using Centriprep 3K filters (Millipore). Deuterated glycine (2 M) was added to the final NMR samples, because this resulted in better long-term stability of the PC4 protein at higher temperatures (*27*). The protein concentration was approximately 0.2−1 mM in all experiments. NMR experiments of the ^{15}N- and ^{13}C/^{15}N-labeled PC4 samples were performed essentially as described in Cavanagh et al. (*34*) at 298 K (or 305 K for enhanced PC4ctd signals) on Varian Inova 500 and 750 MHz and Bruker Avance 500, 600, and 750 MHz spectrometers using triple-resonance probes. Most of the resonances for PC4ctd have been assigned before (*27*) and could be re-assigned for full-length PC4 by overlaying the (^{1}H,^{15}N)-heteronuclear single-quantum coherence (HSQC) spectra of full-length PC4 and PC4ctd and by verification of the nuclear Overhauser enhancement (NOE) patterns from high-resolution 3D NOE spectrometry (NOESY)−(^{1}H,^{15}N)-HSQC spectra. Triple-resonance spectra, 3D HNCACB, 3D HNCO, and 3D HN(CA)CO, of ^{13}C/^{15}N-labeled full-length PC4 have been recorded for the sequential backbone assignment of the ^{1}H, ^{15}N, and ^{13}C resonances from the amino-terminal domain. In addition, 3D total correlation spectroscopy (TOCSY)−(^{1}H,^{15}N)-HSQC and 3D NOESY−(^{1}H,^{15}N)-HSQC spectra have been recorded. Most of the intense peaks in the (^{1}H,^{15}N)-HSQC could be assigned to the residues 3−57 in PC4ntd; however, there is ambiguity for both serine-rich regions. The successive serines 9, 10, 11 and 55, 56, 57 could not be unambiguously assigned because of overlap. However, a combination of results from titration experiments, relaxation studies, and phosphorylation experiments (Jonker et al., manuscript accepted for publication) allowed us to discriminate clearly between the residues from both regions and suggests the reported assignments within these regions. The ^{15}N−T_1 and ^{15}N−$T_{1\rho}$ relaxation experiments at 600 MHz were performed as described by Mulder et al. (*35*). The longitudinal ^{15}N relaxation rates were determined from a series of spectra with delays of 100, 200, 400, 600, 800, 1000, 1200, 1400, and 1600 ms. Relaxation delays used for determining the transversal relaxation rates were 2, 6, 10, 20, 30, 50, 70, 100, 150, and 200 ms, using an off-resonance RF field applied 2000 Hz from the center of the ^{15}N spectrum. To determine the temperature dependence of the backbone ^{1}H and ^{15}N amide chemical shifts, (^{1}H,^{15}N)-HSQC spectra have been recorded in the range from 273 to 303 K. The temperature coefficients were obtained from the slope of the shifts against the temperature by linear fit. The titration experiments were performed by adding increasing amounts (as 1, 5, 10, 20, 40, and 80 μL in total) of concentrated (>1 mM) unlabeled protein or DNA to a 450 μL ^{15}N-labeled PC4 sample (0.2 mM). Both the labeled PC4 protein and the unlabeled target protein are dissolved in the same buffer solution. The titration was ended at an excess of the unlabeled partner, when no significant changes are observed anymore in the (^{1}H,^{15}N)-HSQC spectra after the last addition. The spectrometer was locked on deuterated glycine. Spectra were processed using the software package NMRPipe (*36*) and analyzed using SPARKY 3 (T. D. Goddard and D. G. Kneller, University of California, San Francisco, CA).

RESULTS

Interaction of PC4 with VP16 Depends upon PC4ctd and Is Affected by PC4ntd. PC4 can act as a cofactor for many different transcription activators, and direct interactions with activators have been reported in many cases (*7*, *12*). In parts A and B of Figure 1, we confirm by GST pull-down assays that PC4 can interact with numerous minimal transcription activation domains. Interestingly, the strongest interactions were obtained with the very potent activators VP16 (K_d at 4 °C =90 ± 20 nM for PC4 and 150 ± 80 nM for PC4ctd, data not shown) and E1A (K_d at 4 °C =160 ± 20 nM for PC4 and 450 ± 80 nM for PC4ctd, Figure 1B), while the

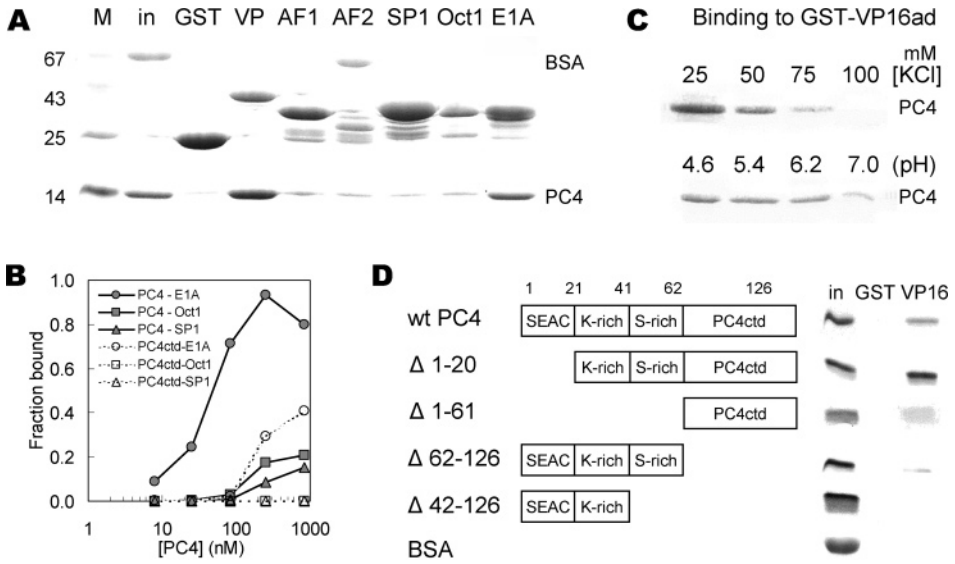

FIGURE 1: (A) Interaction of PC4 with activation domains. GST pull-down assay using 2 μg of the indicated GST fusion proteins. The input lane (in) represents 10% of the total input of both BSA and PC4. Abbreviations: M, marker with the indicated molecular weights (in kilodaltons); VP, activation domain of VP16 (410−490); AF1, human RARβ AF1 (1−76); AF2, human RARβ AF2 (137−448); SP1, human SP1 (139−250); Oct1, human Oct1 (175−269); E1A, adenovirus E1A (121−187). (B) GST pull-down assay at 4 °C using the indicated amounts of PC4 or PC4ctd (in nanomolars) with GST−E1A, GST−Oct1, or GST−SP1. The maximum binding between GST−E1A and PC4 was taken as 1, calculating the other values relative to this maximal interaction. (C) pH and KCl dependence of the interaction between PC4 and VP16ad. (Upper panel) GST pull-down assay using GST−VP16ad and PC4 at different concentrations of KCl (in millimolars) at pH 6.2. (Lower panel) GST pull-down assay using GST−VP16ad and PC4 at the indicated pH in the presence of 50 mM KCl. (D) Domains involved in the interaction between PC4 and VP16ad. In the left panel, a schematic representation is given of the PC4 deletion constructs, with the indicated names, used in the GST pull-down assay with GST−VP16ad. The input lane (in) shows 10% of the total amount of PC4 deletions or BSA added to the reaction, and the GST and VP16ad lanes show the interaction of the proteins with GST and GST−VP16ad, respectively. Abbreviations: SEAC, serine- and acidic-rich region; K-rich, lysine-rich region; S-rich, serine-rich region; PC4ctd, core domain of PC4.

less potent activators displayed (*37*−*40*) weaker interactions with PC4. The interaction between the VP16 activation domain (VP16ad) and PC4 (Figure 1C) as well as the interaction between E1A and PC4 (data not shown) are highly salt-dependent and influenced by pH, indicating that the interactions are predominantly electrostatic in nature. Deletion analysis (Figure 1D) revealed that the amino-terminal domain of PC4 (PC4ntd) alone is unable to interact with VP16ad. However, this region can cooperate with the conserved carboxy-terminal core of the protein (PC4ctd) to increase the interaction of PC4ctd with VP16ad. The SEAC is not required for interaction; instead, a stronger interaction with VP16ad was obtained for the PC4 protein that lacks this region. The relatively weak interactions found between the various activators and PC4 are in good agreement with the relatively broad range of dissociation constants found between transcription activation domains and their targets (*41*−*44*).

The Presence of PC4ntd Differentially Modulates PC4ctd Function. Previous studies suggested that the PC4ntd, in conjugation with the PC4ctd, is involved in dsDNA binding (*9*). The precise role as well as the mechanism underlying the regulation of the PC4 function by its amino-terminal domain is unclear. We show that PC4ntd alone lacks the ability to interact with ssDNA, dsDNA, and VP16ad (Figure 2) and does not possess any helix-destabilizing activity (data not shown). PC4ctd can perform all of these activities albeit with different affinities (Figure 2). Remarkably, the presence of PC4ntd can either be stimulatory (VP16 interaction), neutral (dsDNA), or inhibitory (ssDNA) on the PC4ctd functions. The apparent K_d values at room temperature for the interaction with PC4 and PC4ctd, respectively, are 391 $\pm$ 80 and 991 $\pm$ 195 nM for VP16ad, 55 $\pm$ 33 and 41 $\pm$ 21 nM for dsDNA, and 25 $\pm$ 4 nM and 0.98 $\pm$ 0.23 nM for ssDNA. Whether these in vitro interactions are functionally relevant in vivo remains to be seen; however, the concentration of PC4 in HeLa cell nuclei is estimated to be $\sim$1 μM (*15*), which indicates that these interactions could also occur in vivo. The modulatory role of PC4ntd is further underscored by the observed phosphorylation-dependent increase in ssDNA binding and a decrease in dsDNA and VP16 binding and helix-destabilizing activity of PC4 (Jonker et al., manuscript accepted for publication; *9*, *13*, *15*). The fact that both the presence of the amino-terminal domain and its phosphorylation status influence PC4 functions suggests that PC4ntd (despite the lack of any intrinsic activities) fulfills an important role on the PC4 function. This raises the question of how PC4ntd participates in the PC4ctd-dependent function of the cofactor.

PC4ntd Is an Intrinsically Unstructured Domain. To study the structural characteristics of PC4ntd, NMR spectra were recorded for full-length PC4. The (^{1}H,^{15}N)-HSQC spectrum (Figure 3A) shows a blob of intense amide signals among the well-dispersed peaks that have been assigned to PC4ctd (*27*). The ^{1}H, ^{15}N, and ^{13}C chemical-shift values of these signals, originating from PC4ntd, have been assigned and deposited in the BioMagResBank (accession number 6098). Probability-based secondary-structure identification (PSSI) (*45*), chemical-shift index (CSI) (*46*), and torsion angle likelihood obtained from shift and sequence similarity (TALOS) (*47*) indicate that most of the ^{15}N, ^{1}H, and ^{13}C resonances are around the random-coil positions. The region of residues 16−26 has a tendency toward formation of an α-helical structure and residues 28−42, of a β-strand

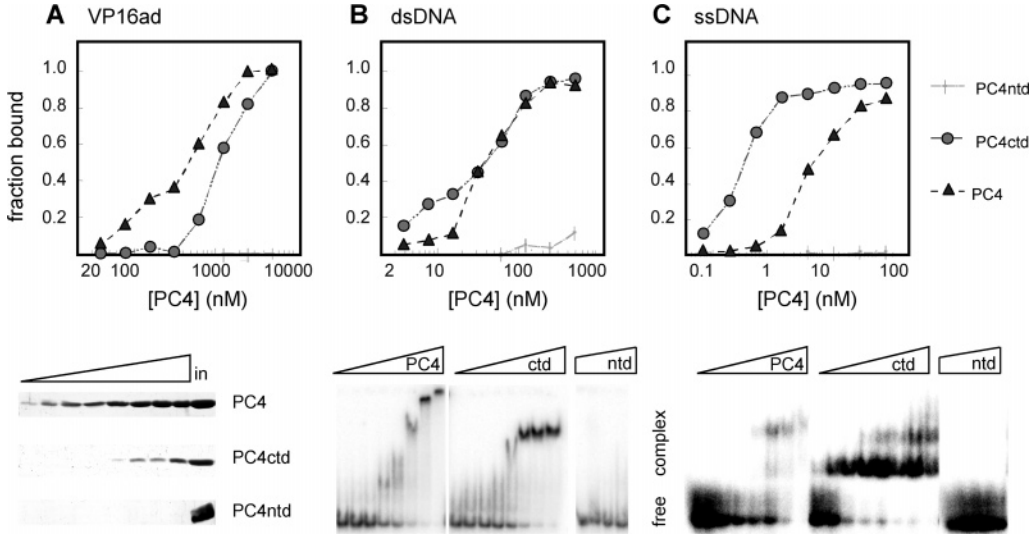

FIGURE 2: Binding properties of PC4, PC4ntd, and PC4ctd to VP16ad, ssDNA, and dsDNA. The upper panel shows a quantification of the interaction of PC4 at room temperature at the indicated concentrations with VP16 using a GST pull-down assay (A) with HIV/ML dsDNA (B) and a 28-bp ssDNA (C) using an EMSA experiment with the indicated amounts of PC4ntd (NTD), PC4ctd (CTD), and full-length PC4. The lower panel shows the Coomassie-stained SDS−PAGE (A) (in, 10% of the total input) or the EMSA autoradiogram (B and C) of the corresponding experiments. Free and complex represent the unbound and PC4-bound DNA, respectively.

structure. This is confirmed by the presence of a substantial number of NOE contacts in 3D NOESY−(^{1}H,^{15}N)-HSQC spectra (data not shown). However, the moderate NOE signal intensities, in combination with the chemical-shift data, indicate that these regions are predominantly unstructured in nature, which suggests either a pliable structure or exchange between the random-coil and more ordered structures. Also upon interaction with VP16ad, we did not observe significant changes in NOE contacts for PC4ntd, which suggest that PC4ntd is highly flexible and mostly unstructured both in the free form and in the complex with the activator. Under identical conditions, we see α-helix formation in the VP16 activation domain (*48*).

PC4ntd Is a Highly Flexible Unstructured Domain. To confirm this flexibility, the dynamical properties of the amino-terminal domain have been analyzed by measuring the heteronuclear relaxation values and the temperature coefficient of the amide proton chemical shifts for full-length PC4 (Supplementary Figure 1 in the Supporting Information). The ^{15}N−$T_{1\rho}$ values for PC4ntd are much higher (∼300 ms) than for the more rigid PC4ctd core domain [∼70 ms (*27*)], indicating higher internal dynamics on the milli−microsecond time scale. Furthermore, the ^{15}N−$T_{1\rho}$ values indicate higher mobility for the SEAC (∼450 ms) than for the rest of PC4ntd. The ^{15}N−T_1 values indicate some enhanced mobility on the pico−nanosecond time scale in the first part of the lysine-rich region (∼20−29), when compared to the rest of PC4ntd. All amide proton chemical shifts of PC4ntd, except for K23 and L24, show a temperature dependence more negative than −4.5 ppb/K, indicating that they are generally not hydrogen-bonded (*49*). The temperature dependence for the amino-terminal end (3−9) and the second part of the lysine-rich region (30−40) is large (± −10 ppb/K) in comparison with the region between residues 10−28 (± −6 ppb/K), suggesting that the amide protons in the latter region are slightly more protected or rigid than in the other regions.

The Two Domains of PC4 Interact Weakly. Despite the absence of an ordered structure, PC4ntd influences the activity of PC4 (Figures 1 and 2). Together with the influence of phosphorylation on PC4 activity (Jonker et al., manuscript accepted for publication), this raises the question of how the presence of PC4ntd differentially modifies PC4 activity. We have recorded (^{1}H,^{15}N)-HSQC spectra of PC4ctd, PC4ntd, and full-length PC4 (Figure 3A) under identical conditions. Although some amide peaks from PC4ctd could not be assigned because of line broadening and spectral overlap with PC4ntd peaks, most resonance differences between full-length PC4 and PC4ctd or PC4ntd were determined (Figure 3B). The presence of PC4ntd causes chemical-shift perturbations in PC4ctd, most prominently in the β1, β2, and the first part of the β3 sheet and moderately within the α helix.

A comparison of the (^{1}H,^{15}N)-HSQC spectra of PC4ntd and full-length PC4 revealed only minor chemical-shift changes for the amide cross-peaks of residues 3−9 and 28−57 (Figure 3B), which suggests an involvement of these regions in the interaction with PC4ctd. The residues in between do not show significant perturbations. The observed chemical-shift perturbations are relatively small but significantly larger than the experimental error (0.003 ppm). Furthermore, titration experiments have been performed where unlabeled PC4ntd or PC4ctd was added to ^{15}N-labeled PC4ctd or PC4ntd, respectively, showing only marginal peak shifts in the (^{1}H,^{15}N)-HSQC spectra (Supplementary Figure 2 in the Supporting Information). These experiments suggest the absence of interactions between the two domains, when present in isolation, arguing that the interaction between both domains is relatively weak and can only be observed when covalently linked. The homogenious behavior of PC4 and PC4ctd are confirmed by gel-filtration experiments at various protein concentrations (Supplementary Figure 3 in the Supporting Information). Furthermore, we did not observe any significant chemical-shift changes or changes in relative intensities between amide signals upon dilution of our PC4 or PC4ctd NMR sample (ranging from 0.1 to 1.5 mM), which indicates that there is no change in the oligomerization state for either PC4 or PC4ctd. Whether this intramolecular domain interaction is of functional

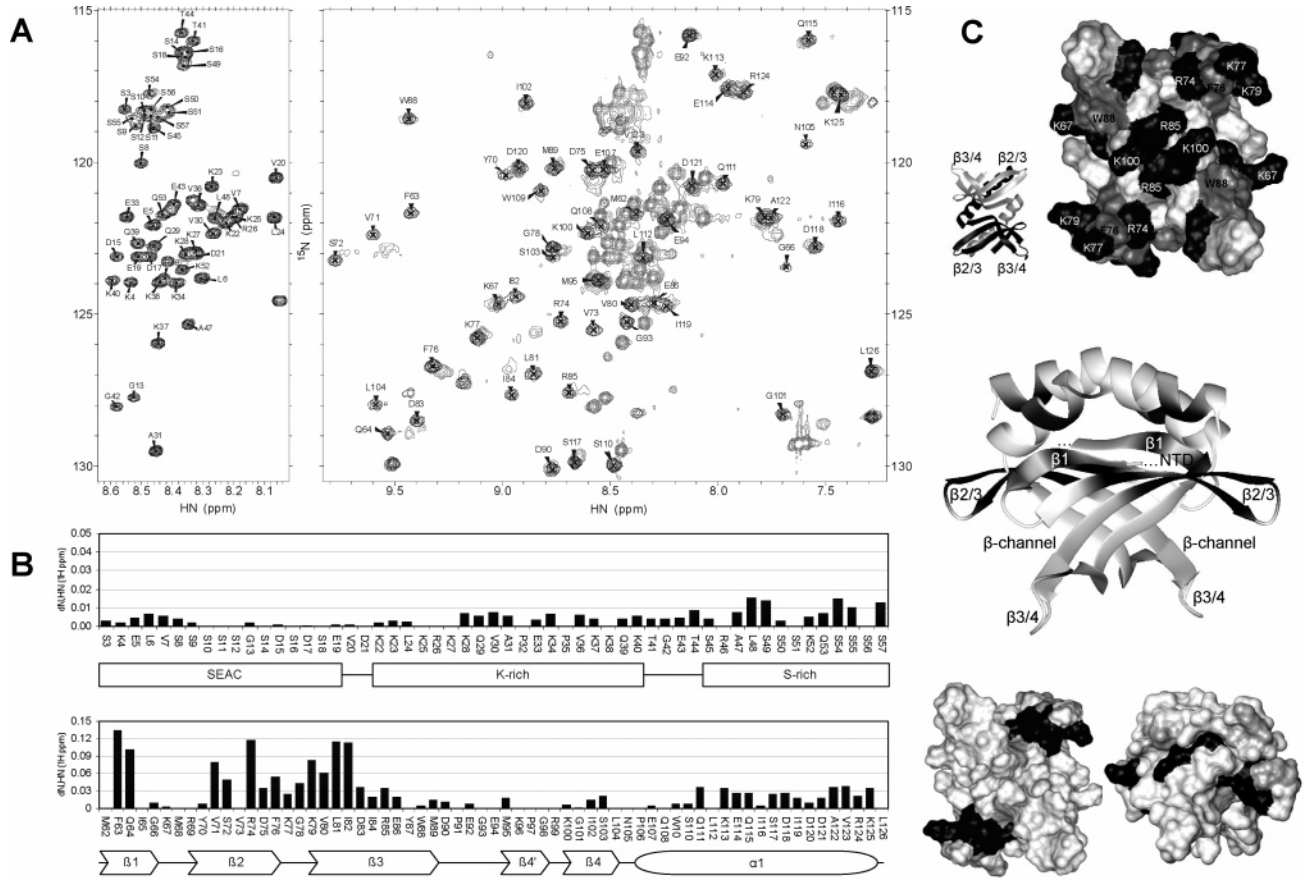

FIGURE 3: Influence of PC4ctd and PC4ntd on each other. (A) Overlay of (^{1}H,^{15}N)-HSQC spectra (500 MHz) of full-length PC4 (gray) with either PC4ntd (left, in black) or PC4ctd (right, in black) in which the amide backbone assignments for either PC4ctd or PC4ntd are indicated. Some peaks (residues G13, G42, G66, G78, G93, G101, S110, and S117) have been folded in the ^{15}N dimension. All spectra were acquired at 305 K in the same buffer solution (400 mM KCl, 50 mM KH_xPO_4 at pH 5.6, and 2 M glycine-d_5). (B) Chemical-shift perturbations in PC4ntd (top panel) or PC4ctd (bottom panel) because of the presence of the other domain. The amide ^{1}H and ^{15}N resonance shifts have been mapped and combined as Euclidian distances between peak maxima, taking into account the gyromagnetic ratio of proton and nitrogen [dN,HN (in ^{1}H ppm) = $\sqrt{((dHN\cdot\gamma HN)^2 + (dN\cdot\gamma N)^2)/\gamma HN}$]. Missing bars indicate that the resonances have not been assigned or could not be traced back in full-length PC4. (C) Surface of the PC4ctd dimer on the top is orientated as indicated by the (black/gray) ribbon diagram next to it and shows the positive-charged residues in black and the hydrophobic residues in gray. Chemical-shift perturbations are presented in black (>0.05 ppm) and dark gray (>0.033 ppm) on the PC4ctd ribbon diagram as well as the surface representations below (the left surface is oriented the same as the one at the top, and the right surface is oriented the same as the PC4ctd ribbon above).

relevance in vivo and is not just the result of the high protein concentrations used in our NMR experiments remains to be seen.

VP16ad and ssDNA Have an Overlapping Binding Surface on the PC4ctd Core Domain. To map the interaction sites for VP16ad on PC4, we performed NMR titration experiments of either ^{15}N-labeled PC4ctd (residues 62−126) or full-length PC4 with unlabeled VP16ad (Figure 4A). The addition of VP16 to PC4 resulted in progressive amide peak shifts, indicative for fast exchange on the NMR time scale and characteristic of a low-affinity complex. Larger chemical-shift perturbations are observed for full-length PC4 when compared with PC4ctd, which is in agreement with the higher binding affinity observed for the first (Figure 2). Significant chemical-shift changes are also observed for the strongly positively charged lysine-rich region (21−48) and the amino-terminal end (3−8 residues) of PC4ntd. Upon the interaction with VP16ad, no peak broadening or decrease of signal intensity is observed for PC4ntd to the extent of PC4ctd and NOE contacts are present in comparable proportions as for PC4 alone (data not shown). These observations exclude the formation of a tight complex between PC4ntd and VP16ad bound to pc4ctd. We suggest that the affected site in PC4ntd might be involved in the electrostatic attraction of VP16ad, bringing the activator in proximity of the PC4ctd interaction surface, thereby affecting the on/off rate of VP16 toward PC4. The ^{15}N−$T_{1\rho}$ values for the backbone nitrogens of PC4ntd decrease by VP16ad complex formation, which is somewhat more pronounced for the lysine-rich region (Supplementary Figure 1 in the Supporting Information). This is most likely due to reduced domain movement and/or the larger size of the complex. The ^{15}N−T_1 values and the temperature coefficient in the first part of the lysine-rich region (∼20−29) are slightly affected by the interaction. The flexibility of this region is reduced by VP16ad complex formation, indicating a PC4ntd-dependent stabilization of the PC4−VP16 complex. Furthermore, a decrease in ^{15}N−T_1 values is observed for the SEAC, which is interpreted as an increase of flexibility for this region because of the loss of contact with PC4ctd.

Surprisingly, the chemical-shift perturbations on PC4ctd, caused by the presence of PC4ntd (Figure 3) and the interaction with VP16ad (Figure 4), overlap partially with the previously published PC4ctd ssDNA-binding site (*27*).

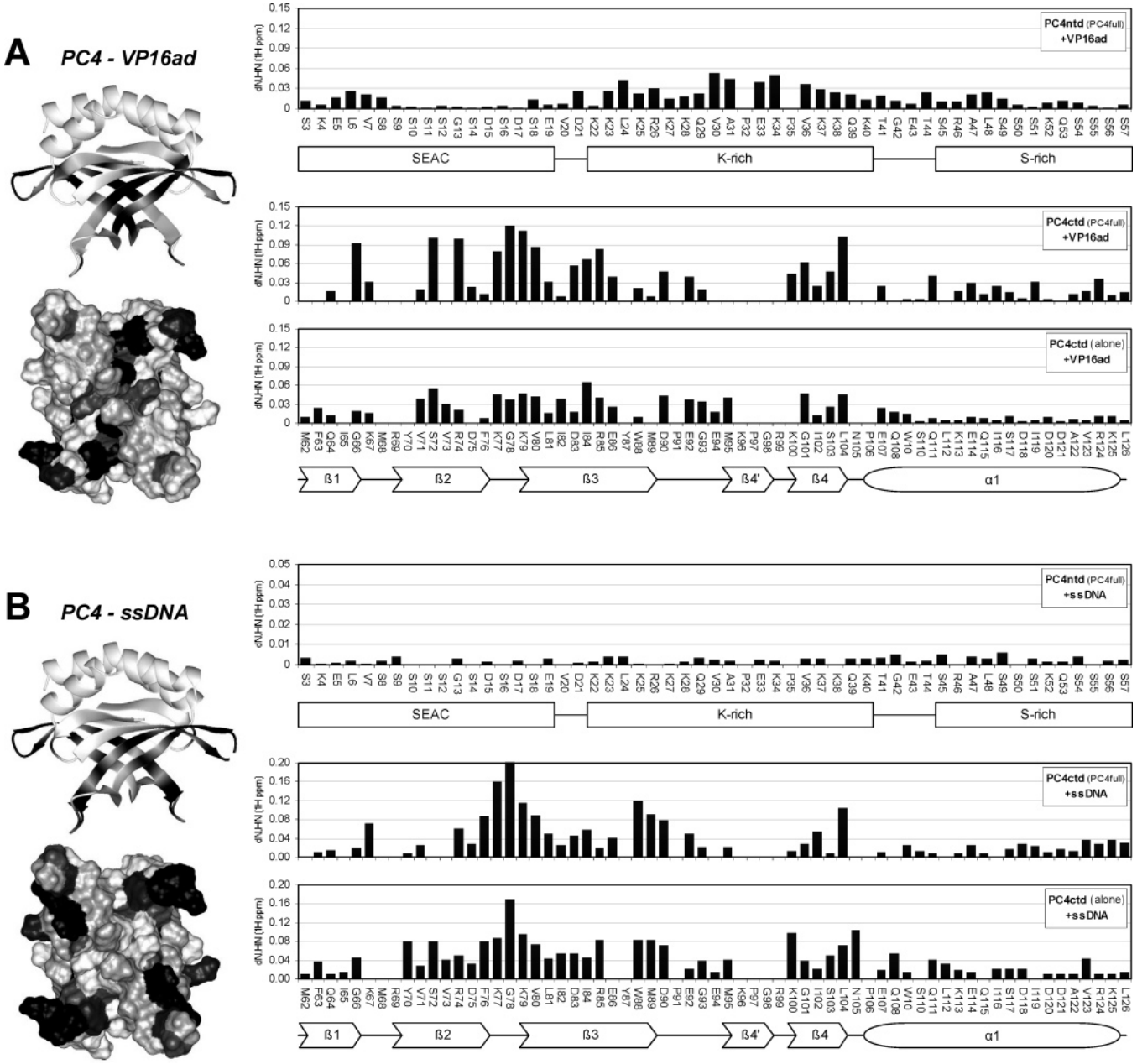

FIGURE 4: Chemical-shift perturbations in PC4 because of the presence of VP16ad or ssDNA. (A) Interaction with VP16ad for full-length PC4 at 305 K and 50 mM KCl and for PC4ctd alone at 400 mM KCl. (B) Interaction with ssDNA for full-length PC4 and PC4ctd (*27*) at 305 K and 400 mM KCl. The amide ^{1}H and ^{15}N resonance shifts have been mapped and combined as Euclidian distances between peak maxima, taking into account the gyromagnetic ratio of proton and nitrogen [dN,HN (in ^{1}H ppm) = $\sqrt{((\mathrm{dHN}\cdot\gamma\mathrm{HN})^2 + (\mathrm{dN}\cdot\gamma\mathrm{N})^2)}/\gamma\mathrm{HN}$]. Missing bars indicate that the resonances have not been assigned or could not be traced back in full-length PC4. In case no unambiguous assignment could be made for the complex state (K77, I84), the minimal perturbation values are shown. The PC4ctd interaction sites (for full-length PC4) are indicated in black (>0.08 ppm) and dark gray (0.04−0.08 ppm) on the ribbon diagrams and surfaces. The orientations are the same as in Figure 3.

To verify the binding of ssDNA to full-length PC4, a titration experiment was performed with the oligonucleotide dT_{18}. The complex formation is in intermediate exchange on the NMR time scale, because most of the amino acids in the ssDNA-binding site show progressive peak shifts of decreasing and increasing signals. The observed chemical-shift perturbations are mapped on the PC4ctd and PC4ntd sequence (Figure 4B). The changes are very similar to that observed by Werten et al. (*27*) for the PC4ctd core domain only and are well in agreement with the recently published X-ray structure of PC4ctd bound to a single-stranded 20-mer oligonucleotide (*50*). The signals originating from PC4ntd do not show any overall chemical-shift perturbations larger than 0.006 ^{1}H ppm, confirming that this region is not involved in the binding to ssDNA (Figure 2).

Both the interactions with VP16ad and ssDNA show particularly large chemical-shift perturbations on the strongly positively charged side of the PC4ctd dimer. The strongest perturbations are observed in the positively charged loop that connects the β2 and β3 sheets, as well as in the β4 sheet region (100−105). While the ssDNA interaction site covers both positively charged residues and hydrophobic residues (F76, W88, and M89) in the β2−β3 and β3−β4 loop regions, the VP16ad interaction appears to affect mainly the positively charged lysine and arginine residues (R74, R85, and K100) in the β channels. In the β1-sheet region, K67 is affected by

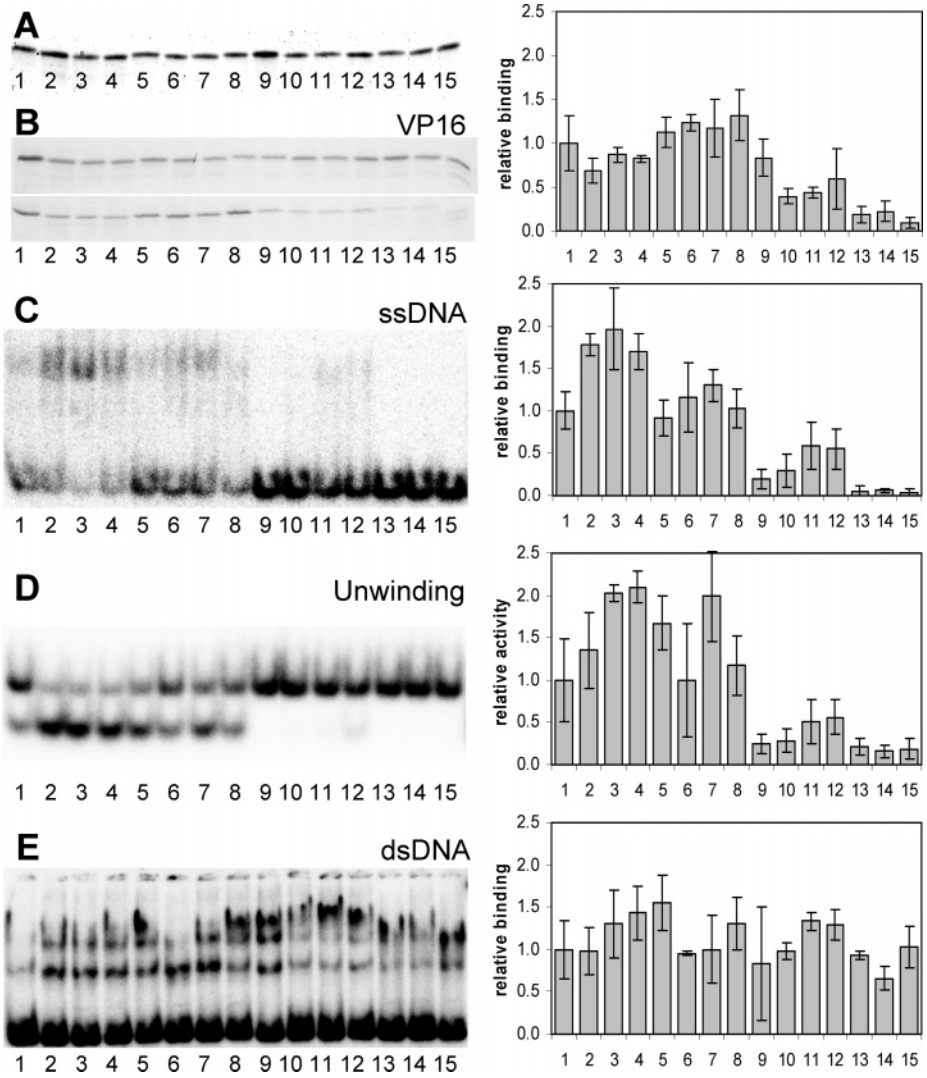

FIGURE 5: Residues of PC4 required for interaction with VP16ad and ssDNA, showing overlap with residues required for unwinding but not with residues involved in the binding to dsDNA. (A) Representative Coomassie-stained SDS−polyacrylamide gel of the mutants used in these binding studies. (B) GST pull-down assay using 2 mg of GST−VP16ad together with 1 mg of PC4. The upper panel shows 10% of the total input of the PC4 mutants, and the lower panel shows the interacting PC4. (C) Interaction of 4 ng of the indicated PC4 mutants with a 28-nucleotide ssDNA. (D) Ability of 100 ng of the indicated PC4 mutants to unwind a melted dsDNA probe (bubble with eight unpaired T residues). (E) Interaction of 40 ng of the indicated PC4 mutants with HIV/ML dsDNA. The left part of the figure shows a representative gel of the interactions or unwinding activities, while the right part of the figure shows the average and standard deviation resulting from the quantification of 3−5 independent experiments. PC4 mutants used: 1, wild-type PC4; 2, K22G,K23G; 3, K25G,R26G; 4, K27G,K28G; 5, K34G; 6, K37G,K38G; 7, A47G,L48G; 8, V20G; 9, K67G; 10, R74G; 11, K77G; 12, K79G; 13, R85G; 14, K100G; and 15, β2−β3 (F76A,K77G,K79G).

ssDNA, while only a large perturbation of the amide resonances of the neighboring G66 residue is observed upon the interaction with VP16ad.

Determination of PC4 Residues Involved in VP16ad and ssDNA Binding and DNA Unwinding. The interaction between PC4 and VP16 is negatively influenced by salt and strongly dependent on pH (Figure 1C). Furthermore, the most significant chemical-shift changes upon the interaction with either ssDNA or VP16 occur at the positively charged amino acids or their neighboring residues. These observations led us to conclude that these charged residues are critically involved in both interactions. To confirm the electrostatic driven interaction of PC4 with VP16 and ssDNA and investigate the binding with dsDNA, point mutants were expressed and purified (Figure 5A). All lysine or arginine residues that show significant chemical-shift changes by the addition of ssDNA or VP16 were mutated to glycine, either single or in pairs of two residues at a time. Furthermore, V20 was mutated to investigate whether the side chain of this valine is essential in the connection between SEAC and the lysine-rich region. The double mutant A47G,L48G was designed because of substantial chemical-shift changes for these two residues upon the interaction with VP16. Finally, the previously described triple mutant in the β2−β3 loop (F76A/K77G/K79G) was used as a control (*15*).

GST pull-down assays of GST−VP16ad with the PC4 mutants (Figure 5B) revealed that the carboxy-terminal core domain is most important for the interaction. Except for K67, all of the mutated residues in PC4ctd contribute to the VP16 interaction, which is in agreement with the minor chemical-shift changes of this residue as monitored by NMR. None of the mutants completely lost the ability to interact with VP16, indicating that multiple interactions contribute to this complex. This observation fits with the relatively mild effect

of the mutation of individual or pairs of negatively charged VP16 residues on transcription (*51*, *52*) and interaction with PC4 (*48*). Although the PC4ntd is not essential for the interaction, it clearly has a modulatory role. The positively charged residues 22,23, 25,26, and 27,28 contribute to the interaction. The mutation of the lysine residues 34 and 37,-38 and the hydrophobic residues 47 and 48 does not affect the interaction, despite the large chemical-shift perturbations observed by NMR.

EMSAs using ssDNA (Figure 5C) revealed, as expected (*27*), that only residues within the conserved core of the protein participate in the interaction with ssDNA and bubble DNA (data not shown). None of the mutants completely block binding, although the phenotype for R85 and K100 is almost as severe as the $\beta2-\beta3$ mutant, which is essentially devoid of ssDNA-binding activity (*15*). Except for K67, all residues required for VP16 binding also affect ssDNA binding, which is in agreement with the NMR titration experiments. Strikingly, the same PC4ntd residues that positively contributed to the PC4−VP16 interaction had a negative effect on the interaction between PC4 and ssDNA.

DNA-unwinding experiments revealed that the same residues influencing ssDNA binding participate in the helix destabilization activity (Figure 5D). The modulatory role for PC4ntd, as observed for the other interactions, is underscored by the small increase in unwinding activity upon the mutation of the lysine residues within the amino-terminal domain and reflects the higher unwinding activity of PC4ctd in comparison with full-length PC4.

Residues R99 and K100 in PC4ctd are Essential for dsDNA Binding. In NMR titration experiments using full-length ^{15}N-labeled PC4 and oligonucleotides of either 28 or 60 base pairs of dsDNA, we observed resonance shifts accompanied with a fast decrease in PC4ctd amide signal intensity and peak broadening (data not shown). This prevented us from identifying the PC4ctd interaction surface for dsDNA. The observed peak broadening indicates the formation of a large protein−DNA complex, reminiscent of the high-order complexes formed in the EMSA experiments (Figure 2B). However, for PC4ntd, hardly any decrease of signal intensity is detected and only some small chemical-shift changes (0.015 ^{1}H ppm) and splitting of peaks are observed in the first part of the lysine-rich region. This indicates that PC4ntd is only marginally involved, while PC4ctd is essential for dsDNA complex formation.

To determine the dsDNA-binding surface, we investigated the ability of PC4 mutants to bind to dsDNA (Figure 5E). None of the mutated PC4 proteins dramatically affected the interaction with dsDNA. Most residues in PC4ntd that contribute to the VP16ad interaction and negatively influence ssDNA binding also have a small contribution in dsDNA binding, because mutation of these residues to glycine results in a somewhat higher binding affinity. A small but significant decrease was obtained for K100G. Brandsen et al. (*26*) suggested before that dsDNA binding could be accomplished in a tetrameric arrangement of PC4 dimers in which a critical role was suggested for R99. Quantification of the dsDNA-binding affinities of wild-type PC4, R99G, and K100G (Figure 6) revealed a 4-fold increase in K_d for these point mutants. This is at least in part due to an increase in the k_{off} because these complexes appeared less stable, evidenced by smearing of the protein−DNA complex. The double mutant

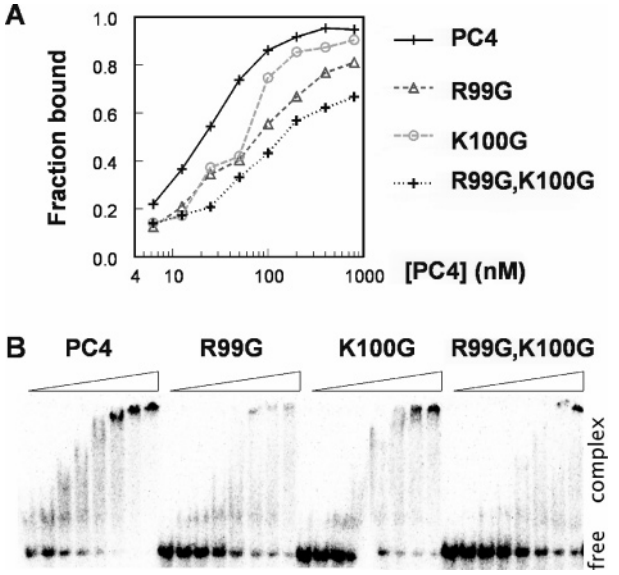

FIGURE 6: Binding of PC4 to dsDNA is dependent upon residues R99 and K100. (A) Quantification of dsDNA binding of the indicated concentrations (in nanomolars) of PC4 and point mutants to the HIV/ML probe. (B) Autoradiogram of the corresponding experiments. Free and complex represent the unbound and PC4-bound DNA, respectively.

R99G,K100G has at least a 10-fold lower affinity for dsDNA, and no binding saturation was detected at the highest protein concentration (1 μM). The mutation of these residues to either glutamate or alanine gave similar binding affinities (data not shown). Not surprisingly, also the ssDNA binding, helix destabilization, and VP16 interaction were significantly decreased or abolished for the R99 and K100 mutants (Figures 5 and 6 and data not shown).

Interaction with VP16 Affects the DNA-Binding and DNA-Unwinding Activities of PC4. The remarkable overlap in the surface area of PC4 required for interaction with VP16ad or DNA led us to suggest that these interactions are mutually exclusive. To test this hypothesis, EMSAs were performed using dsDNA and ssDNA in the absence or presence of an excess of VP16ad (parts A and B of Figure 7). A 2-fold decrease in DNA-binding affinity was observed in the presence of VP16. More importantly, the DNA-unwinding activity of PC4 was almost completely lost in the presence of the VP16 activation domain (Figure 7C). The PC4 concentration required for half-maximal activity increased at least 40-fold, while at the highest concentrations tested (4 mM), activity was at least 10 times lower. At a 1 mM concentration of PC4 (Figure 7D), a large decrease in unwinding activity is already observed at a molar ratio of roughly 8:1 (monomeric PC4/VP16). In a parallel DNA-binding experiment (data not shown), we observed similar binding of PC4 to the substrate in the presence or absence of VP16, arguing that VP16 blocks the unwinding activity, without significantly interfering with the ability to bind to bubble DNA. Furthermore, the interaction between PC4 and VP16ad can be destroyed by the addition of a molar excess of either ssDNA or dsDNA (Figure 7E), with the former being slightly more effective than the latter, which reflects the higher affinities of PC4 toward ssDNA [Figure 2 (*9*, *15*)]. The relatively lower molar excess of DNA required for the disturbance of the PC4−VP16 interaction in GST pull-down assays in comparison with the molar excess of VP16 required

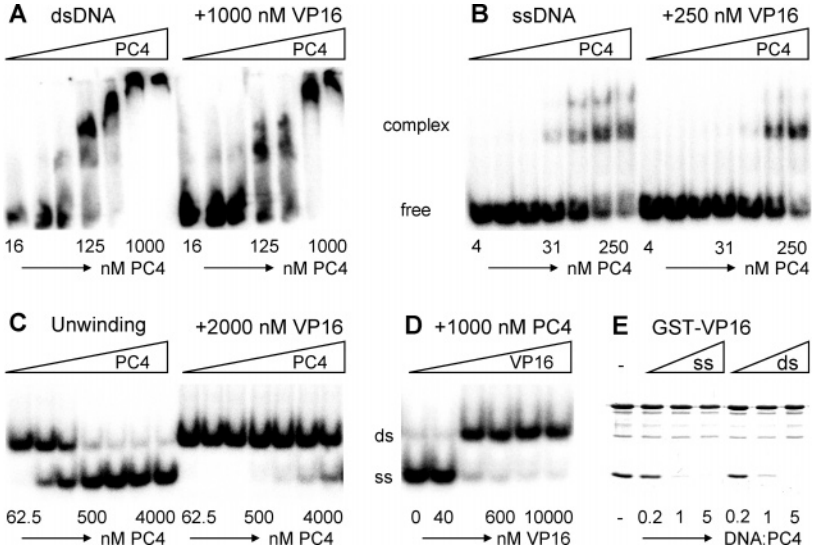

FIGURE 7: Competitive binding of VP16ad and DNA to PC4 and the influence of VP16ad on the DNA-unwinding activity. (A) Interaction of the indicated amount of PC4 (16, 31, 62.5, 125, 250, 500, or 1000 nM) with dsDNA (HIV/ML) in the absence or presence of 1000 nM VP16ad. The assay was performed under low-salt conditions. (B) Interaction using 4, 8, 16, 31, 62.5, 125, or 250 nM PC4 with ssDNA (BCTC) as a probe in the absence or presence of 250 nM VP16ad, performed under low-salt conditions. (C) Unwinding reaction using 62.5, 125, 250, 500, 1000, 2000, or 4000 nM of PC4 with a bubble as a substrate (eight unpaired bases) in the absence or presence of 2000 nM VP16ad. (D) Unwinding reaction using 1000 nM PC4 in the presence of 0, 40, 150, 600, 2500, or 10 000 nM VP16ad with a bubble as a substrate. (E) GST pull-down assay using 2 μg of GST−VP16ad in a GST pull-down assay buffer with 1 μM PC4 without the competitor (−) or with ssDNA (BCTC) or dsDNA (BCTC + BGAG) in a molar ratio of DNA/PC4 of 0.2, 1, and 5.

to compete for PC4−DNA complexes in EMSA experiments is due to the much lower affinity of PC4 to VP16 compared to DNA substrates (Figure 2).

DISCUSSION

The function, if any, of unstructured regions and their relation to the more structured regions in proteins is largely unknown. Through functional characterization of the various biochemical activities performed by PC4, we found that both type of regions, which each constitute approximately half of the protein, fulfill a specific role. The structured part (PC4ctd) is required and sufficient for all interactions tested, while the unstructured part (PC4ntd) has a more regulatory role. The structure of PC4ctd is well-defined and contains partially overlapping DNA- and VP16ad-binding sites. As a consequence, binding of PC4 to DNA or VP16 is mutually exclusive. NMR data indicate that PC4ntd is highly flexible and mostly unstructured and also when PC4 is in complex with VP16ad. Nevertheless, PC4ntd stimulates interactions with activators and negatively affects the ssDNA-binding and DNA-unwinding activity of PC4ctd. A comparison of the NMR spectra between PC4 and PC4ctd and PC4ntd in isolation revealed significant shifts in both PC4ntd (3−9 and 28−57) and PC4ctd. Interestingly, these residues are part of the ssDNA and VP16ad interaction surface. We propose transient and dynamic interdomain interactions between the unstructured PC4ntd and structured PC4ctd overlapping with the ssDNA/VP16ad interaction surface that affects the cofactor activities of PC4.

Binding Models of PC4ctd to ssDNA, dsDNA, and VP16ad. NMR and biochemical data revealed that PC4ctd is the most essential part, directly involved in the DNA-unwinding activity and binding to VP16ad, dsDNA, and ssDNA. The interaction surfaces for VP16ad and ssDNA have been determined (Figures 4 and 5) and show a partial overlap (Figures 4 and 8), which excludes simultaneous binding and indicates competitive binding of PC4 to either ssDNA or VP16ad. In agreement with this, biochemical experiments indicate that the interaction of PC4 with VP16ad decreases the binding affinity toward DNA and strongly affects the DNA-unwinding activity (Figure 7). The binding of VP16ad to PC4 is dependent on the salt concentration and pH (Figure 1C). The PC4 interaction site for the negatively charged VP16ad and ssDNA is strongly positively charged, indicating a predominantly electrostatic binding mode. However, also specific hydrophobic residues are involved. Using the homology between the ssDNA-binding surface of the RPA−ssDNA complex (1JMC, *53*) and the β-sheet region of PC4ctd, we made a model for the PC4−ssDNA complex. Similarly, using an ambiguity-driven docking approach (Haddock, *54*), on the basis of NMR titration and site-directed mutagenesis data, we proposed a model for the PC4−VP16ad interations (*48*). The ssDNA-binding site covers most of the β2−β3 and β3−β4 loop regions, while the VP16ad-binding site mostly resides in the β channels. A major difference in the largely overlapping interaction site is the involvement of K67 in the interaction with ssDNA but not with VP16ad.

Brandsen et al. observed two different tetrameric arrangements of PC4ctd dimers in their crystal packing. The charge distribution suggested to them that an arrangement involving contacts between the β3−β4 loops would permit dsDNA binding. In this orientation, the tetramer of PC4 dimers is wrapped around B-DNA, whereby it was proposed that R99 was interacting with the phosphate backbone. We show here that this residue together with K100 is essential for dsDNA binding. With some side-chain rearrangements or local rearrangements, the latter residue could also contact the phosphate backbone. Although other binding models could be proposed, the lack of any contribution to dsDNA binding of the other positively charged residues (Figure 5) supports this model. In the crystal packing, the PC4 tetramer of dimers

is not closed; therefore, a continuous stretch of PC4 dimers wrapped around dsDNA can be easily accomplished, which explains the observed higher order complex formation in NMR and EMSA experiments. The presence of such higher order structures was confirmed by analytical gel-filtration experiments and native gel electrophoresis both free and in the presence of DNA (data not shown). The residues R99 and K100 also contribute to ssDNA and VP16ad binding, explaining the observed competition for binding (Figure 7).

An Intrinsically Unstructured Domain Influences PC4 Activity. The extended amino-terminal tail of PC4 can be phosphorylated (*9*, *31*) and acetylated (*28*), which regulates the interactions with activators and DNA. In addition, it has been shown that this region can inhibit cdk-mediated phosphorylation of RNA polymerase II (*29*). Deletion analysis (Figures 1D and 2) revealed that PC4ntd alone is unable to interact with VP16ad, ssDNA, or dsDNA. While its presence only marginally influences dsDNA binding, it stimulates the interaction of PC4ctd with the activator and negatively modulates ssDNA binding (Figures 2 and 5). Although some moderate NOE signal intensities, chemical-shift values, temperature coefficients, and relaxation data suggest the presence of unstable structure elements in the lysine-rich region and flanking residues, PC4ntd is highly flexible and mostly unstructured. This characteristic is comparable with the absence of a structure for transcription activation domains (TADs). Most TADs adopt a well-ordered conformation upon the interaction with their target. Remarkably, we found no direct or indirect evidence from NOE data or relaxation measurements for the formation of a more ordered structure for PC4ntd upon the interaction with DNA or VP16ad. At present, we cannot exclude that upon the interaction with other targets PC4ntd could adopt a more ordered conformation, although we fail to see such changes also with a different class of TADs: SP1 and Oct1 (data not shown). We present here two distinct models that explain how the intrinsically unstructured tail influences the activity of the structured PC4 core.

PC4ntd Dependent Influence on PC4ctd through the Direct Interaction with Target Molecules. NMR titration experiments indicated that the lysine-rich region is significantly affected by the interaction with VP16ad (Figure 4). We propose that this region stimulates binding to VP16ad by enlarging the positively charged interaction surface. The overall decrease of $^{15}N-T_{1\rho}$ relaxation rates is somewhat more pronounced in the lysine-rich region, which indicates reduced domain movement and/or formation of a larger complex. Although the whole region is affected by the interaction, $^{15}N-T_1$ relaxation data and the temperature coefficient of the amide chemical shifts indicate that, in agreement with VP16ad titration experiments and mutagenesis data (Figure 5), the first part of the lysine-rich region (residues 20−29) is most important for the interaction with the VP16 activation domain. The flexibility of this part of the lysine-rich region is somewhat reduced upon VP16ad complex formation, indicating that this region may decrease the VP16ad off rate by stabilizing the PC4ctd−VP16ad interaction. Changes in the structural properties are not observed. Both the type of interactions and the modification-dependent regulation of interactions are similar to what has been observed for the histone tail DNA interactions within the nucleosome (*55*−*57*). Whether such interactions are also contributing to PC4−dsDNA interactions is presently unclear. The mutation of individual lysine residues as well as the deletion of the complete PC4ntd only marginally influence dsDNA binding. NMR titration data also indicate that PC4ntd is not significantly influenced by the presence of dsDNA. Remarkably, dsDNA binding is diminished by CKII-dependent phosphorylation of the serine-rich domain of PC4ntd by a yet to be determined mechanism.

Dynamic Functional Regulation of PC4ctd Mediated by Interactions with PC4ntd. Despite the absence of a direct interaction between ssDNA and PC4ntd (Figure 4B), the presence of this unstructured tail negatively influences the ssDNA-binding affinity of PC4ctd. We propose that this is caused by a transient interaction between PC4ntd and PC4ctd, on the basis of differences in the (^1H,^{15}N)-HSQC spectra of full-length PC4, PC4ctd, and PC4ntd. Next to the expected changes in the carboxy terminus of the PC4ntd that is in contact with the PC4ctd core, differences are observed for the residues 3−9 of the SEAC (Figure 3). Furthermore, chemical-shift differences between the (^1H,^{15}N)-HSQC spectra of full-length PC4 and PC4ctd (Figure 3) clearly indicate structural or environmental changes in the PC4ctd core domain because of the presence of PC4ntd. The localization of the PC4ntd-dependent chemical-shift changes in PC4ctd suggest that at least part of the ssDNA and VP16ad interaction surface is influenced by the presence of PC4ntd. The involvement of the SEAC is underscored by the observation that deletion of the amino-terminal SEAC increases the interaction between PC4 and VP16ad (Figure 1), and also the interaction with ssDNA is stronger (K. Kaiser, unpublished observations) in comparison with full-length PC4. Furthermore, the PC4 cofactor function is mediated by CKII-mediated phosphorylation of serine residues in this region (*9*). On the basis of chemical-shift changes (Figure 4) and increased flexibility in the first part of the SEAC upon the interaction with VP16ad (Supplementary Figure 1 in the Supporting Information), we propose that the negatively charged SEAC and the acidic VP16ad bind competitively to the positively charged PC4ctd surface. The different structural properties of the flexible PC4ntd and PC4ctd core both in isolation and in complex with the activator or DNA exclude the formation of a tight complex. Therefore, we propose a transient interaction between both domains, which might reduce the ssDNA-binding affinity and the unwinding activity because of competitive binding and/or steric hindrance. Similar observations have been made for TFIIB, in which the amino-terminal domain (TFIIBn) shields part of the surface in the carboxy-terminal core domain (TFIIBc), which is important for the interaction with VP16ad or the TBP−TATA complex (*58*). Furthermore, the ssDNA-binding human replication protein A (RPA70) has some functional resemblance to PC4 and is also composed of a structured domain and an unstructured flexible tail (*59*). The global β-barrel fold of RPA contains a basic cleft, which might be involved in binding to acidic activator proteins. It was recently shown that phosphorylation of the tail induces intersubunit interactions between the negatively charged tail and the basic cleft of RPA and modulates the interactions with dsDNA (*60*), in a manner reminiscent to what we observe for PC4.

Functional Consequences of PC4ntd-Dependent Interactions for PC4 Cofactor Activity. Figure 8 shows a schematic

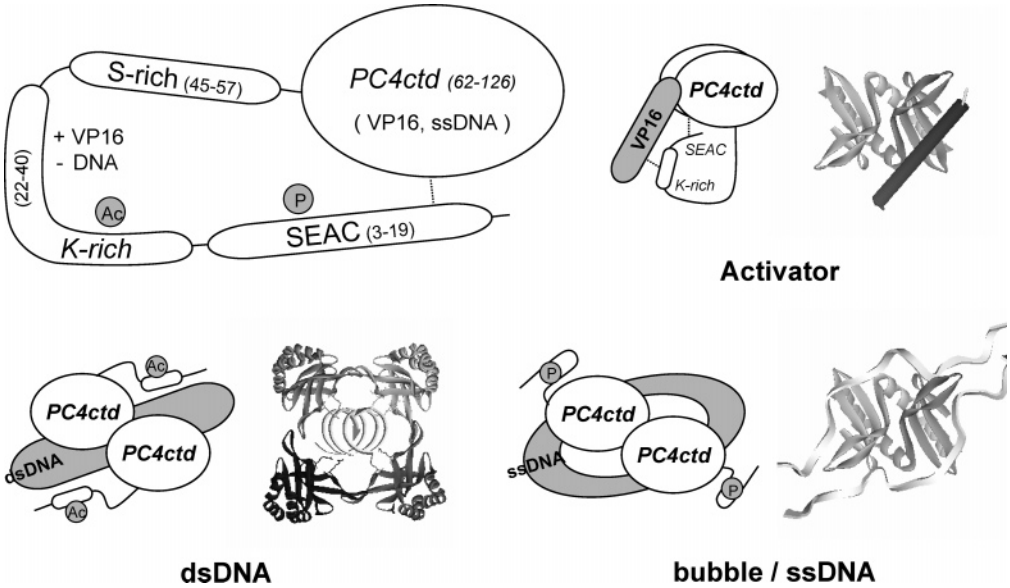

FIGURE 8: Schematic models of the modulatory and regulatory role of PC4ntd on PC4ctd and models based on NMR titrations, mutagenesis, and docking, describing the binding to the activator VP16, dsDNA, and ssDNA. The lysine-rich region (and residues flanking this region) is involved in binding to VP16ad and affects the DNA-binding properties. The first part of the SEAC contacts PC4ctd and has a negative effect on the VP16ad-binding affinity. Acetylation increases the dsDNA-binding affinity (*28*). The SEAC can be phosphorylated, which affects the cofactor function in many aspects (*9*, *11*, *31*).

model for the structural and functional aspects of PC4ntd. The amino-terminal tail of PC4 is highly flexible and mostly unstructured. The flexibility of the protein chain appears essential for its function, most likely allowing modifications (phosphorylation and acetylation) and enabling both intra- and intermolecular interaction to the structured core and/or transcription factors. We do not observe the formation of a rigid tertiary structure of PC4ntd when PC4 binds to VP16ad or DNA. The intrinsic plasticity allows the flexible PC4ntd to adopt various conformations, which permits regulation of the various PC4 cofactor functions. The observation that the PC4ctd core domain is affected by the presence of PC4ntd and vice versa (Figure 3) suggests that PC4ntd fulfills its function by transient interactions with PC4ctd. The strength or presence of these interactions can be modulated by chemical modifications, thereby explaining the influence of PC4ntd on PC4ctd activity despite the lack of any intrinsic activity of the PC4ntd by itself.

ACKNOWLEDGMENT

We thank S. Werten and P.C. van der Vliet for providing the plasmids and H. van Aken for DNA sequencing. We also thank S.H.W. Scheres for useful discussions and his efforts to elucidate the full length PC4 structure by X-ray crystallography. This work is supported by financial assistance from The Netherlands Organization for Scientific Research (NWO).

SUPPORTING INFORMATION AVAILABLE

Supplementary Figure 1, heteronuclear relaxation rates, $^{15}N-T_1$ (A) and $^{15}N-T_{1\rho}$ (B), and the temperature coefficient (C) of the amide chemical shifts (273−303 K) of PC4ntd in the free form and with an excess of VP16ad; Supplementary Figure 2, chemical-shift perturbations in PC4ntd (top panel) or PC4ctd (bottom panel) observed in titration experiments with the other domain; Supplementary Figure 3, gel-filtration experiment of full-length PC4 and PC4ctd. This material is available free of charge via the Internet at http://pubs.acs.org.

REFERENCES

1. Wright, P. E., and Dyson, H. J. (1999) Intrinsically unstructured proteins: Re-assessing the protein structure−function paradigm, *J. Mol. Biol. 293*, 321−331.
2. Dunker, A. K., Lawson, J. D., Brown, C. J., Williams, R. M., Romero, P., Oh, J. S., Oldfield, C. J., Campen, A. M., Ratliff, C. M., Hipps, K. W., Ausio, J., Nissen, M. S., Reeves, R., Kang, C., Kissinger, C. R., Bailey, R. W., Griswold, M. D., Chiu, W., Garner, E. C., and Obradovic, Z. (2001) Intrinsically disordered protein, *J. Mol. Graphics Modell. 19*, 26−59.
3. Struhl, K. (1996) Chromatin structure and RNA polymerase II connection: Implications for transcription, *Cell 84*, 179−182.
4. Roeder, R. G. (1996) The role of general initiation factors in transcription by RNA polymerase II, *Trends Biochem. Sci. 21*, 327−335.
5. Orphanides, G., Lagrange, T., and Reinberg, D. (1996) The general transcription factors of RNA polymerase II, *Genes Dev. 10*, 2657−2683.
6. Verrijzer, C. P., and Tjian, R. (1996) TAFs mediate transcriptional activation and promoter selectivity, *Trends Biochem. Sci. 21*, 338−342.
7. Kaiser, K., and Meisterernst, M. (1996) The human general co-factors, *Trends Biochem. Sci. 21*, 342−345.
8. Burley, S. K., and Roeder, R. G. (1996) Biochemistry and structural biology of transcription factor IID (TFIID), *Annu. Rev. Biochem. 65*, 769−799.
9. Kaiser, K., Stelzer, G., and Meisterernst, M. (1995) The coactivator p15 (PC4) initiates transcriptional activation during TFIIA−TFIID−promoter complex formation, *EMBO J. 14*, 3520−3527.
10. Gu, W., Malik, S., Ito, M., Yuan, C. X., Fondell, J. D., Zhang, X., Martinez, E., Qin, J., and Roeder, R. G. (1999) A novel human SRB/MED-containing cofactor complex, SMCC, involved in transcription regulation, *Mol. Cell 3*, 97−108.
11. Malik, S., Guermah, M., and Roeder, R. G. (1998) A dynamic model for PC4 coactivator function in RNA polymerase II transcription, *Proc. Natl. Acad. Sci. U.S.A. 95*, 2192−2197.
12. Ge, H., and Roeder, R. G. (1994) Purification, cloning, and characterization of a human coactivator, PC4, that mediates transcriptional activation of class II genes, *Cell 78*, 513−523.
13. Kretzschmar, M., Kaiser, K., Lottspeich, F., and Meisterernst, M. (1994) A novel mediator of class II gene transcription with

homology to viral immediate-early transcriptional regulators, *Cell 78*, 525−534.
14. Wu, S. Y., and Chiang, C. M. (1998) Properties of PC4 and an RNA polymerase II complex in directing activated and basal transcription in vitro, *J. Biol. Chem. 273*, 12492−12498.
15. Werten, S., Stelzer, G., Goppelt, A., Langen, F. M., Gros, P., Timmers, H. Th. M., van der Vliet, P. C., and Meisterernst, M. (1998) Interaction of PC4 with melted DNA inhibits transcription, *EMBO J. 17*, 5103−5111.
16. Kershnar, E., Wu, S. Y., and Chiang, C. M. (1998) Immunoaffinity purification and functional characterization of human transcription factor IIH and RNA polymerase II from clonal cell lines that conditionally express epitope-tagged subunits of the multiprotein complexes, *J. Biol. Chem. 273*, 34444−34453.
17. Wu, S. Y., Kershnar, E., and Chiang, C. M. (1998) TAFII-independent activation mediated by human TBP in the presence of the positive cofactor PC4, *EMBO J. 17*, 4478−4490.
18. Fukuda, A., Tokonabe, S., Hamada, M., Matsumoto, M., Tsukui, T., Nogi, Y., and Hisatake, K. (2003) Alleviation of PC4-mediated transcriptional repression by the ERCC3 helicase activity of general transcription factor TFIIH, *J. Biol. Chem. 278*, 14827−14831.
19. Calvo, O., and Manley, J. L. (2001) Evolutionarily conserved interaction between CstF-64 and PC4 links transcription, polyadenylation, and termination, *Mol. Cell 7*, 1013−1023.
20. Pan, Z. Q., Ge, H., Amin, A. A., and Hurwitz, J. (1996) Transcription-positive cofactor 4 forms complexes with HSSB (RPA) on single-stranded DNA and influences HSSB-dependent enzymatic synthesis of simian virus 40 DNA, *J. Biol. Chem. 271*, 22111−22116.
21. Haile, D. T., and Parvin, J. D. (1999) Activation of transcription in vitro by the BRCA1 carboxyl-terminal domain, *J. Biol. Chem. 274*, 2113−2117.
22. Kannan, P., and Tainsky, M. A. (1999) Coactivator PC4 mediates AP-2 transcriptional activity and suppresses ras-induced transformation dependent on AP-2 transcriptional interference, *Mol. Cell. Biol. 19*, 899−908.
23. Ballard, D. W., Philbrick, W. M., and Bothwell, A. L. (1988) Identification of a novel 9-kDa polypeptide from nuclear extracts. DNA binding properties, primary structure, and in vitro expression, *J. Biol. Chem. 263*, 8450−8457.
24. Soma, G., Kitahara, N., and Andoh, T. (1984) Molecular cloning and characterization of a cDNA clone for a protein specifically expressed in embryo as well as in a chemically induced pancreatic B cell tumor of rat, *Biochem. Biophys. Res. Commun. 124*, 164−171.
25. Lacoste, J., Codani-Simonart, S., Best-Belpomme, M., and Peronnet, F. (1995) Characterization and cloning of p11, a transrepressor of *Drosophila melanogaster* retrotransposon 1731, *Nucleic Acids Res. 23*, 5073−5079.
26. Brandsen, J., Werten, S., van der Vliet, P. C., Meisterernst, M., Kroon, J., and Gros, P. (1997) C-terminal domain of transcription cofactor PC4 reveals dimeric ssDNA binding site, *Nat. Struct. Biol. 4*, 900−903.
27. Werten, S., Wechselberger, R., Boelens, R., van der Vliet, P. C., and Kaptein, R. (1999) Identification of the single-stranded DNA binding surface of the transcriptional coactivator PC4 by NMR, *J. Biol. Chem. 274*, 3693−3699.
28. Kumar, B. R., Swaminathan, V., Banerjee, S., and Kundu, T. K. (2001) p300-mediated acetylation of human transcriptional coactivator PC4 is inhibited by phosphorylation, *J. Biol. Chem. 276*, 16804−16809.
29. Schang, L. M., Hwang, G. J., Dynlacht, B. D., Speicher, D. W., Bantly, A., Schaffer, P. A., Shilatifard, A., Ge, H., and Shiekhattar, R. (2000) Human PC4 is a substrate-specific inhibitor of RNA polymerase II phosphorylation, *J. Biol. Chem. 275*, 6071−6074.
30. Dahmus, M. E. (1996) Reversible phosphorylation of the C-terminal domain of RNA polymerase II, *J. Biol. Chem. 271*, 19009−19012.
31. Ge, H., Zhao, Y., Chait, B. T., and Roeder, R. G. (1994) Phosphorylation negatively regulates the function of coactivator PC4, *Proc. Natl. Acad. Sci. U.S.A. 91*, 12691−12695.
32. Folkers, G. E., and van der Saag, P. T. (1995) Adenovirus E1A functions as a cofactor for retinoic acid receptor β (RAR β) through direct interaction with RAR β, *Mol. Cell. Biol. 15*, 5868−5878.
33. Werten, S., Langen, F. W., van Schaik, R., Timmers, H. Th. M., Meisterernst, M., and van der Vliet, P. C. (1998) High-affinity DNA binding by the C-terminal domain of the transcriptional coactivator PC4 requires simultaneous interaction with two opposing unpaired strands and results in helix destabilization, *J. Mol. Biol. 276*, 367−377.
34. Cavanagh, J., Fairbrother, W. J., Palmer, A. G., III, and Skelton, N. J. (1996) *Protein NMR Spectroscopy*; Academic Press, San Diego, CA.
35. Mulder, F. A. A., de Graaf, R. A., Kaptein, R., and Boelens, R. (1998) An off-resonance rotating frame relaxation experiment for the investigation of macromolecular dynamics using adiabatic rotations, *J. Magn. Reson. 131*, 351−357.
36. Delaglio, F., Grzesiek, S., Vuister, G. W., Zhu, G., Pfeifer, J., and Bax, A. (1995) NMRPipe: A multidimensional spectral processing system based on UNIX pipes, *J. Biomol. NMR 6*, 277−293.
37. Sadowski, I., Ma, J., Triezenberg, S., and Ptashne, M. (1988) GAL4-VP16 is an unusually potent transcriptional activator, *Nature 335*, 563−564.
38. Lillie, J. W., and Green, M. R. (1989) Transcription activation by the adenovirus E1a protein, *Nature 338*, 39−44.
39. Seipel, K., Georgiev, O., and Schaffner, W. (1992) Different activation domains stimulate transcription from remote ("enhancer") and proximal ("promoter") positions, *EMBO J. 11*, 4961−4968.
40. Folkers, G. E., van der Leede, B. J., and van der Saag, P. T. (1993) The retinoic acid receptor-β 2 contains two separate cell-specific transactivation domains, at the N-terminus and in the ligand-binding domain, *Mol. Endocrinol. 7*, 616−627.
41. Chi, S. W., Lee, S. H., Kim, D. H., Ahn, M. J., Kim, J. S., Woo, J. Y., Torizawa, T., Kainosho, M., and Han, K. H. (2005) Structural details on mdm2−p53 interaction, *J. Biol. Chem. 280*, 38795−38802.
42. Nedialkov, Y. A., and Triezenberg, S. J. (2004) Quantitative assessment of in vitro interactions implicates TATA-binding protein as a target of the VP16C transcriptional activation region, *Arch. Biochem. Biophys. 425*, 77−86.
43. Paal, K., Baeuerle, P. A., and Schmitz, M. L. (1997) Basal transcription factors TBP and TFIIB and the viral coactivator E1A 13S bind with distinct affinities and kinetics to the transactivation domain of NF-κB p65, *Nucleic Acids Res. 25*, 1050−1055.
44. Burakov, D., Wong, C. W., Rachez, C., Cheskis, B. J., and Freedman, L. P. (2000) Functional interactions between the estrogen receptor and DRIP205, a subunit of the heteromeric DRIP coactivator complex, *J. Biol. Chem. 275*, 20928−20934.
45. Wang, Y., and Jardetzky, O. (2002) Probability-based protein secondary structure identification using combined NMR chemical-shift data, *Protein Sci. 11*, 852−861.
46. Wishart, D. S., and Sykes, B. D. (1994) The ^{13}C chemical-shift index: A simple method for the identification of protein secondary structure using ^{13}C chemical-shift data, *J. Biomol. NMR 4*, 171−180.
47. Cornilescu, G., Delaglio, F., and Bax, A. (1999) Protein backbone angle restraints from searching a database for chemical shift and sequence homology, *J. Biomol. NMR 13*, 289−302.
48. Jonker, H. R. A., Wechselberger, R. W., Boelens, R., Folkers, G. E., and Kaptein, R. (2005) Structural properties of the promiscuous VP16 activation domain, *Biochemistry 44*, 827−839.
49. Baxter, N. J., and Williamson, M. P. (1997) Temperature dependence of ^{1}H chemical shifts in proteins, *J. Biomol. NMR 9*, 359−369.
50. Werten, S., and Moras, D. (2006) A global transcription cofactor bound to juxtaposed strands of unwound DNA, *Nat. Struct. Mol. Biol. 13*, 181−182.
51. Seipel, K., Georgiev, O., and Schaffner, W. (1994) A minimal transcription activation domain consisting of a specific array of aspartic acid and leucine residues, *Biol. Chem. Hoppe-Seyler 375*, 463−470.
52. Cress, W. D., and Triezenberg, S. J. (1991) Critical structural elements of the VP16 transcriptional activation domain, *Science 251*, 87−90.
53. Bochkarev, A., Pfuetzner, R. A., Edwards, A. M., and Frappier, L. (1997) Structure of the single-stranded-DNA-binding domain of replication protein A bound to DNA, *Nature 385*, 176−181.
54. Dominguez, C., Boelens, R., and Bonvin, A. M. (2003) HADDOCK: A protein−protein docking approach based on biochemical or biophysical information, *J. Am. Chem. Soc. 125*, 1731−1737.

55. Wu, J., and Grunstein, M. (2000) 25 years after the nucleosome model: Chromatin modifications, *Trends Biochem. Sci. 25*, 619−623.
56. Kornberg, R. D., and Lorch, Y. (1999) Twenty-five years of the nucleosome, fundamental particle of the eukaryote chromosome, *Cell 98*, 285−294.
57. Berger, S. L. (2001) An embarrassment of niches: The many covalent modifications of histones in transcriptional regulation, *Oncogene 20*, 3007−3013.
58. Hayashi, F., Ishima, R., Liu, D., Tong, K. I., Kim, S., Reinberg, D., Bagby, S., and Ikura, M. (1998) Human general transcription factor TFIIB: Conformational variability and interaction with VP16 activation domain, *Biochemistry 37*, 7941−7951.
59. Jacobs, D. M., Lipton, A. S., Isern, N. G., Daughdrill, G. W., Lowry, D. F., Gomes, X., and Wold, M. S. (1999) Human replication protein A: Global fold of the N-terminal RPA-70 domain reveals a basic cleft and flexible C-terminal linker, *J. Biomol. NMR 14*, 321−331.
60. Binz, S. K., Lao, Y., Lowry, D. F., and Wold, M. S. (2003) The phosphorylation domain of the 32-kDa subunit of replication protein A modulates RPA−DNA interactions: Evidence for an intersubunit interaction, *J. Biol. Chem. 278*, 35584−35591.

BI052531B